


Article

Characteristic Length Scale during the Time Evolution of a Turbulent Bose-Einstein Condensate

Lucas Madeira^{1,*} , Arnol D. García-Orozco¹, Michelle A. Moreno-Armijos¹, Francisco Ednilson Alves dos Santos² and Vanderlei S. Bagnato^{1,3}

¹ Instituto de Física de São Carlos, Universidade de São Paulo, CP 369, São Carlos, São Paulo, Brazil

² Departamento de Física, Universidade Federal de São Carlos, São Carlos 13565-905, Brazil

³ Hagler Fellow, Hagler Institute for Advanced Study, Texas A&M University, College Station, Texas 77843, USA

* Correspondence: madeira@ifsc.usp.br

Abstract: Quantum turbulence is characterized by many degrees of freedom interacting non-linearly to produce disordered states, both in space and time. The advances in trapping, cooling, and tuning the interparticle interactions in atomic Bose-Einstein condensates (BECs) make them excellent candidates for studying quantum turbulence. In this work, we investigate the decaying regime of quantum turbulence in a trapped BEC. Although much progress has been made in understanding quantum turbulence, other strategies are needed to overcome some intrinsic difficulties. We present an alternative way of investigating this phenomenon by defining and computing a characteristic length scale, which possesses relevant characteristics to study the establishment of the quantum turbulent regime. One intrinsic difficulty related to these systems is that absorption images of BECs are projected to a plane, thus eliminating some of the information present in the original momentum distribution. We overcome this difficulty by exploring the symmetry of the cloud, which allows us to reconstruct the three-dimensional momentum distributions with the inverse Abel transform. We present our analysis with both the two- and three-dimensional momentum distributions, discussing their similarities and differences. We argue that the characteristic length allows us to visualize the time evolution of the turbulent state intuitively.

Keywords: quantum turbulence; Bose-Einstein condensate; out-of-equilibrium

1. Introduction

Turbulence is a process that occurs in many types of fluids and a wide range of length scales. The field of quantum turbulence (QT) deals with turbulence in quantum fluids, such as liquid helium and trapped Bose-Einstein condensates (BECs) [1–3]. Its classical counterpart, classical turbulence, is a process that occurs in fluids spanning the climatic effects that involve large masses down to capillaries. It is characterized by many degrees of freedom interacting non-linearly to produce disordered states, both in space and time. Turbulence presents properties that are universal, regardless of the system under consideration. Many aspects of classical turbulence are not well-understood, so dealing with its quantum version, quantum turbulence, seems very ambitious. However, turbulence in quantum fluids might be more manageable than its classical counterpart because the vortex circulation is quantized in the former and continuous for classical fluids. Additionally, the advances in trapping, cooling, and tuning the interparticle interactions in atomic BECs make them excellent candidates for studying quantum turbulence and connecting it to related fields [4].

Much progress has been made in understanding and characterizing QT since the first observation of turbulence in a trapped BEC and its signature self-similar expansion [5,6]. A breakthrough was the identification of a particle cascade, which appears as a power-law in the momentum distribution [7,8],

$$n(k) \propto k^{-\delta}, \quad (1)$$



Citation: Lastname, F.; Lastname, F.; Lastname, F. Title. *Preprints* **2021**, *1*, 0. <https://doi.org/>

Received:

Accepted:

Published:

Publisher's Note: MDPI stays neutral with regard to jurisdictional claims in published maps and institutional affiliations.

where δ is a positive constant, and its value depends on the mechanism behind the generation of the turbulent state.

However, there are some intrinsic difficulties in determining the range and exponent of the power-law. The range of length scales and, consequently, momentum scales available in trapped BEC experiments is very narrow compared to other systems (superfluid helium, for example). Additionally, different theoretical models predict close together exponents, and experiments do not yet have the necessary precision to distinguish between them. Hence, approaches other than the power-law behavior have been employed to overcome these issues. Energy and particle fluxes have been used in simulations [9,10] and experiments [11, 12] to overcome some of these difficulties. Since turbulence and disorder are intimately related, an approach based on the entropy of turbulent BECs has also been successfully applied [13] as an alternative method to investigate and characterize quantum turbulence.

A typical scale used to study turbulence in liquid helium is the vortex line density. Its time dependence provides evidence of the mechanism behind the turbulent regime [14]. In some ^4He experiments, where visualization techniques are well-developed, the geometry and interactions of vortices can be directly observed [15]. In trapped BECs, where the range of length scales available is much smaller, the visualization techniques have not yet reached the same level of detail.

In this work, we employed a length scale associated with the momentum distribution $n(k)$ to study the onset of turbulence and the turbulent state. It is inspired by the integral length scale, which is a quantity commonly used in classical turbulence. If we assume isotropic flow, then the integral length scale L_E can be written in terms of the incompressible kinetic energy spectrum $E(k)$ [16–18],

$$L_E(t) \propto \frac{\int_0^\infty dk E(k, t)/k}{\int_0^\infty dk E(k, t)}. \quad (2)$$

Casting Eq. (2) in this form also illustrates that it is the length scale that contains most of the energy of the system.

It is known from numerical simulations that in some cases turbulence is mainly in the form of waves, and other cases mainly in the form of vortices, depending on the excitation protocol and boundary conditions of the system. Since moving vortices radiate waves and strong waves can create vortices, the relative proportion of waves and vortices depends on the particular experiment. In numerical simulations, one has access to the phase of the wave function. Thus the circulation can be computed to distinguish vortices from waves. Moreover, in the simulations, one can formally identify the compressible kinetic energy, which comes from waves, and the incompressible kinetic energy related to vortices. Unlike in the simulations, in the experiments we cannot separate waves and vortices so easily.

However, with current experimental techniques we can measure the momentum distribution $n(k)$ independently of its origin: waves, vortices or a combination of both. Hence, with Eq. (2) in mind, we define the following length scale,

$$L(t) = \frac{\int_0^\infty dk n(k, t)/k}{\int_0^\infty dk n(k, t)}. \quad (3)$$

Intuitively, L is associated with the scale where most of the particles reside. In this work, we investigated the behavior of this quantity, and we showed it is possible to use it to study a turbulent BEC.

Besides the difficulties mentioned above, there is also an experimental challenge when studying QT in trapped BECs. The momentum distribution of the cloud is obtained using a two-dimensional (2D) projection of the three-dimensional (3D) condensate. We employed the inverse Abel transform, an integral transform that connects the 2D projection of an axially or spherically symmetric function to its 3D value, to reconstruct the momentum distribution of the three-dimensional cloud. We showed that the results for the characteristic length scale are qualitatively the same if calculated using the two-dimensional projection.

This indicates that it is possible to study some aspects of the turbulent states using the experimental data directly, without reconstructing the three-dimensional cloud.

This work is structured as follows. First, we provide the experimental details of how the BECs are produced and excited. Then we present the momentum distributions both in two and three dimensions. These are used to compute the characteristic length scale and other quantities related to it. We discuss both the implications of our findings regarding the length scale and the projection of the cloud. In the Appendix, we provide the Abel transforms of momentum distributions relevant to our system.

2. Experimental Procedure

The first step is the production of a Bose-Einstein condensate, containing approximately 4×10^5 ^{87}Rb atoms in the hyperfine state $|F, m_F\rangle = |2, 2\rangle$, confined in a Quadrupole-Ioffe configuration (QUIC) magnetic trap of frequencies $\omega_r/2\pi = 130.7(8)$ Hz and $\omega_x/2\pi = 21.8(2)$ Hz. Before any excitation is applied, the unperturbed BEC has a condensate fraction of 70(5)%, the chemical potential at the center of the cloud is $\mu_0/k_B = 124(5)$ nK, and the healing length corresponds to $\xi_0 = 0.15(2)$ μm . Details of the experimental procedure and other technical remarks can be found in previous works [6,13,19,20].

In Fig. 1(a) we present schematically the protocol we employed to drive the BEC out of equilibrium. After the condensate is produced, while it is still trapped, an oscillating magnetic field is applied. The excitation potential is given by $V_{\text{exc}}(\mathbf{r}, t) = A[1 - \cos(\Omega t)]x'/R_x$, where $R_x = 42$ μm is the in-trap extent of the BEC along the x -axis of the trap. The field is produced by a pair of anti-Helmholtz coils placed with their axis tilted by a small angle (approximately 5°) with respect to the axis of the trap. Since the perturbation is not aligned with the axes of the condensate, the oscillations generate deformations, displacements, and rotations. Several excitation parameters can be varied, such as the amplitude A , time, and perturbation frequency. In this work, we perform the parametric excitation of fixed frequency $\Omega/(2\pi) = 132.8$ Hz, which is close to the radial trapping frequency.

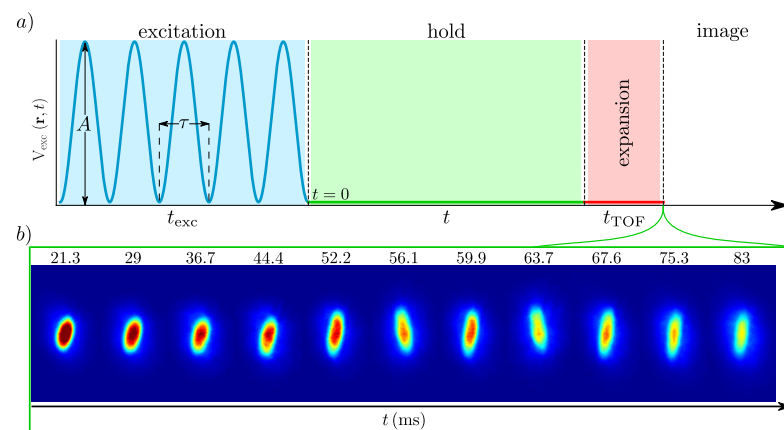


Figure 1. (a) Schematic representation of the excitation protocol. The experiment begins with the production of an unperturbed BEC in the trap. Then, a sinusoidal potential of amplitude A and period τ is applied during t_{exc} . The system evolves during a time t , after which the trap is released, and an absorption image is taken after a time-of-flight t_{TOF} . (b) Absorption images for an excitation amplitude of $A = 1.8 \mu_0$ as a function of the holding time.

The excitation amplitude is increased until an amplitude is reached where the momentum distribution corresponds to an out-of-equilibrium state with turbulent characteristics. The excitation time also varies since there is a compromise between the excitation time and the amplitude to generate the turbulent state. For instance, larger amplitudes need less time to reach similar conditions than it would take for smaller amplitudes. The range of amplitudes and excitation times to obtain a turbulent state was the topic of investigation in previous works [6,19,20]. The excitation protocol is applied during a time $t_{\text{exc}} = 5\tau$, where $\tau = 2\pi/\Omega$. The amplitude A is varied, ranging from 0 (no perturbation) to $2.2\mu_0$.

After the excitation is turned off, the atomic cloud is held for a time t inside the trap, which is varied from 20 to 90 ms, leading to the temporal evolution of the momentum distribution $n(k, t)$. Then, we turn off the trap potential and measure $n(k, t)$ using absorption images taken from the ballistic expansion of the cloud after a time of flight (TOF) of $t_{\text{TOF}} = 30$ ms. In Fig. 1(b), we show typical absorption images corresponding to an excitation amplitude of $A = 1.8 \mu_0$ for different holding times t .

For each excitation amplitude and holding time we perform several realizations of the experiment, and then average the results. In Fig. 2 we show a typical two-dimensional momentum distribution obtained from the absorption images. The distance that an atom has traveled from the center of the cloud is given by $r = \hbar t_{\text{TOF}} k / m$, where \hbar is Planck's constant and m is the atomic mass. Thus, the TOF technique corresponds to a Fourier transform of the spatial distribution, which yields the momentum distribution, $n(r) \propto n(\hbar t_{\text{TOF}} k / m)$. There are known shortcomings of the TOF technique, which do not significantly impact our momentum distributions. Most investigations concerning the limitations of the TOF measurements assume that the interaction energy exceeds (or at least is of the same order as) the kinetic component. However, the turbulent state is kinetically dominated, which means that the interaction energy plays a small role in the effects of a turbulent cloud [21]. Hence, this technique has been used successfully to obtain the momentum distribution of turbulent trapped BECs [7,8].

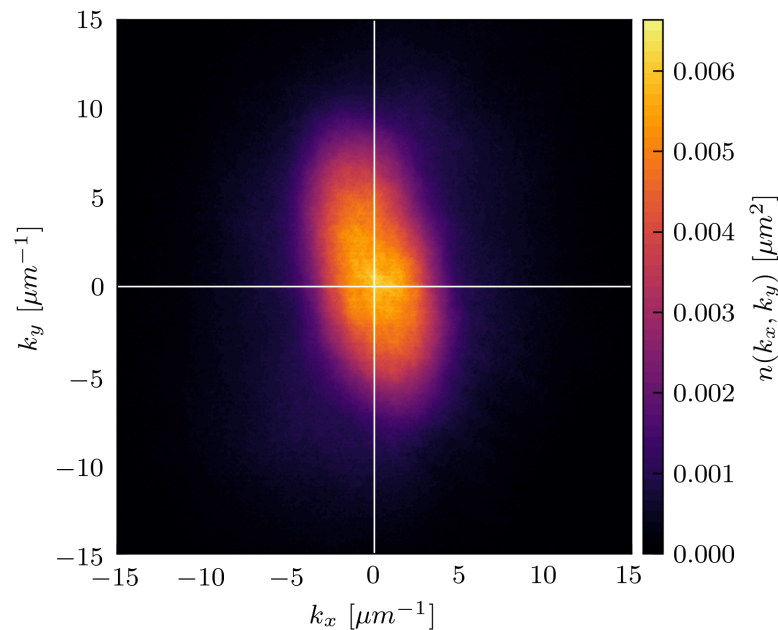


Figure 2. Momentum distribution $n(k_x, k_y)$ obtained from the absorption images of the cloud for an excitation of amplitude $A = 1.8 \mu_0$ and $t = 36.7$ ms.

3. Momentum distributions

We performed angular averages on the momentum distributions $n(k_x, k_y, t)$ obtained from the absorption images, such that the resulting profiles depend only on $k = (k_x^2 + k_y^2)^{1/2}$. The two-dimensional momentum distributions $n_{2D}(k, t)$ are normalized according to

$$2\pi \int dk k n_{2D}(k, t) = 1. \quad (4)$$

As discussed above, an experimental challenge when studying momentum distributions of trapped BECs is that the absorption images correspond to a projection of the cloud. We overcome this difficulty by considering the symmetry of the trapped BEC in momentum space. The inverse Abel transform [22] has been successfully used in the literature [7,8] to

obtain the 3D momentum distribution from its two-dimensional projection. It is an integral transform given by

$$n_{3D}(k, t) = -\frac{1}{\pi} \int_k^\infty \frac{dn_{2D}(k', t)}{dk'} \frac{dk'}{\sqrt{k'^2 - k^2}}. \quad (5)$$

We normalized the distributions according to

$$4\pi \int dk k^2 n_{3D}(k, t) = 1. \quad (6)$$

The signature of a particle cascade is a power-law, $n(k) \propto k^{-\delta}$. Equations (4) and (6), together with dimensional analysis, suggest that if we observe a power-law both in the two-dimensional momentum distribution, $n_{2D}(k) \propto k^{-\delta_{2D}}$, and in the three-dimensional one, $n_{3D}(k) \propto k^{-\delta_{3D}}$, then their exponents differ by one, $\delta_{3D} - \delta_{2D} = 1$. To go beyond simple dimension analysis, in Appendix A we derive this relation analytically for the case where a power-law is present over all k -range. Although this toy-model is nonphysical, it sheds light on how we can reconstruct the three-dimensional momentum distribution based on symmetry arguments.

In our system, the low-momenta region of $n(k)$ is dominated by the presence of the condensate, which corresponds to a Gaussian distribution. We show in Appendix A that the inverse Abel transform of a Gaussian function is also a Gaussian with the same width. This symmetry is extremely useful because we can work with the two-dimensional projections for quantities related to the Gaussian shape without the need for 3D reconstruction. This is the case of the temperature, which is related to the width of the Gaussian.

All the arguments presented above indicate that the power-law exponents in an ideal situation would be related through $\delta_{3D} - \delta_{2D} \approx 1$. However, the fact that we have the power-law behavior superimposed with the condensate at the low-momenta region of the momentum distribution alters this relation. Hence, we need to verify the exponents with the experimental data.

We performed the experiment employing 6 different excitation amplitudes. Only for the three highest ones, $A=1.8, 2.0$, and $2.2 \mu_0$, we observed the appearance of a power-law. In Fig. 3 we present the momentum distributions for an excitation amplitude of $A=1.8 \mu_0$ (which are qualitatively the same for $A=2.0$ and $2.2 \mu_0$). Around $t \approx 35$ ms and in the region $10 \mu\text{m}^{-1} \leq k \leq 15 \mu\text{m}^{-1}$, we observe the establishment of a power-law behavior characteristic of a turbulent cloud. We found the exponents $\delta_{2D} = 3.1(1)$ and $\delta_{3D} = 3.8(2)$, which lead to $\delta_{3D} - \delta_{2D} = 0.7(3)$. It is interesting to see that even in our finite-sized non-homogeneous system inside an anisotropic trap we still have $\delta_{3D} - \delta_{2D}$ close to one.

4. The characteristic length scale

We computed the characteristic length scale given by Eq. (3) using the experimental data available,

$$\begin{aligned} L_{2D}(t) &= \frac{\int_{k_D}^{k_d} dk n_{2D}(k, t)}{\int_{k_D}^{k_d} dk k n_{2D}(k, t)} = 2\pi \int_{k_D}^{k_d} dk n_{2D}(k, t), \\ L_{3D}(t) &= \frac{\int_{k_D}^{k_d} dk k n_{3D}(k, t)}{\int_{k_D}^{k_d} dk k^2 n_{3D}(k, t)} = 4\pi \int_{k_D}^{k_d} dk k n_{3D}(k, t), \end{aligned} \quad (7)$$

where $k_D \sim 0.05 \mu\text{m}^{-1}$ and $k_d \sim 30 \mu\text{m}^{-1}$ are the smallest and largest k we can measure, respectively.

Using the momentum distributions obtained with different excitation amplitudes and holding times, we can study the time evolution of the BEC, ranging from a slightly perturbed cloud up to a turbulent state. In Fig. 4 we present our results for the characteristic length scale computed both with the two-dimensional projection of the cloud and its three-

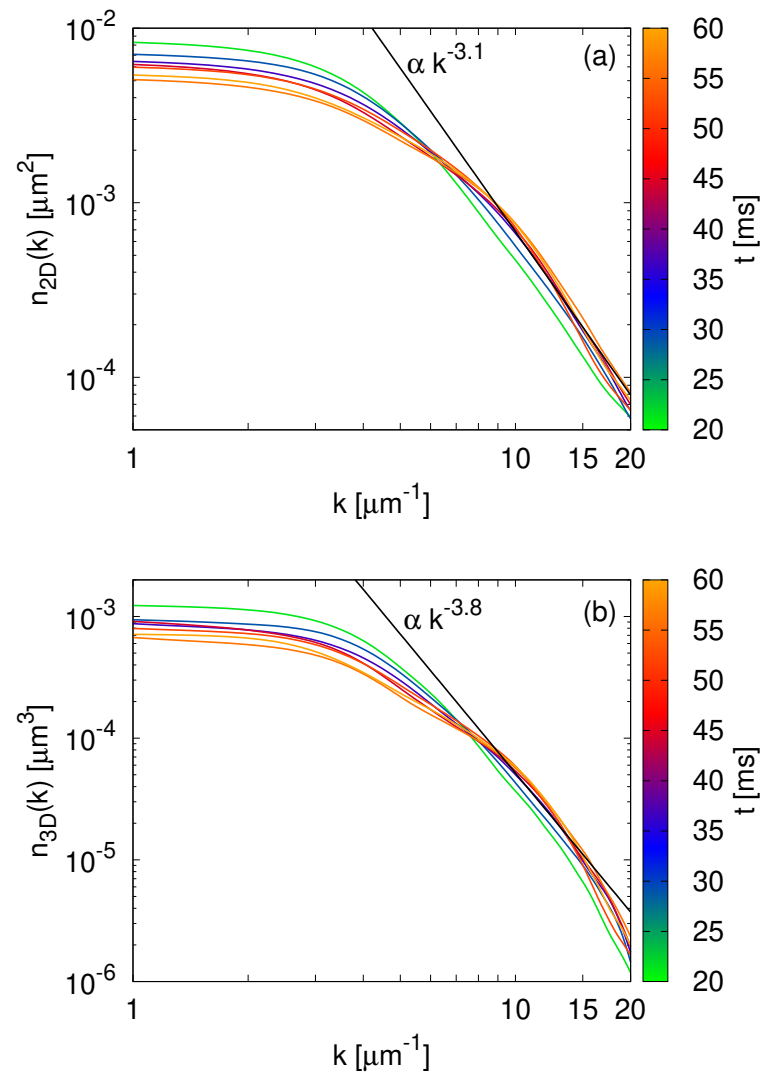


Figure 3. Time evolution of the momentum distributions for an excitation amplitude of $A=1.8 \mu_0$. We present the results obtained with both (a) the angular average of the absorption image and (b) the three-dimensional reconstruction of the cloud using the inverse Abel transform. In both plots, we include the curve corresponding to the power-law behavior characteristic of the turbulent states as a guide to the eye.

dimensional reconstruction. Although they differ quantitatively, their qualitative behavior is remarkably the same.

The $L(t)$ value can be interpreted as the evolution of the length scale where most of the particles are located. If we think of $1/k$ as being a weight in Eq. (3), then $L(t)$ is related to the inverse of the momentum value for which $n(k)/k$ is peaked. Nucleation of excitations occurs during the excitation, whether in the form of vortices or waves. Then the interaction of these excitations takes place, leading to different stages of deviation from equilibrium.

For small excitation amplitudes, $A = 0.8 \mu_0$, the system is only slightly disturbed and removed from equilibrium, but it does not have enough energy to reach what is considered a disordered state. In this case, it evolves differently from the others, and the value of L is approximately constant with time.

For intermediate perturbations, $A = 1.4$ and $1.6 \mu_0$, there is a separation between these results and the smallest amplitude, besides a clear dependence with time. For these excitation amplitudes, we are in a regime best characterized as the onset of turbulence.

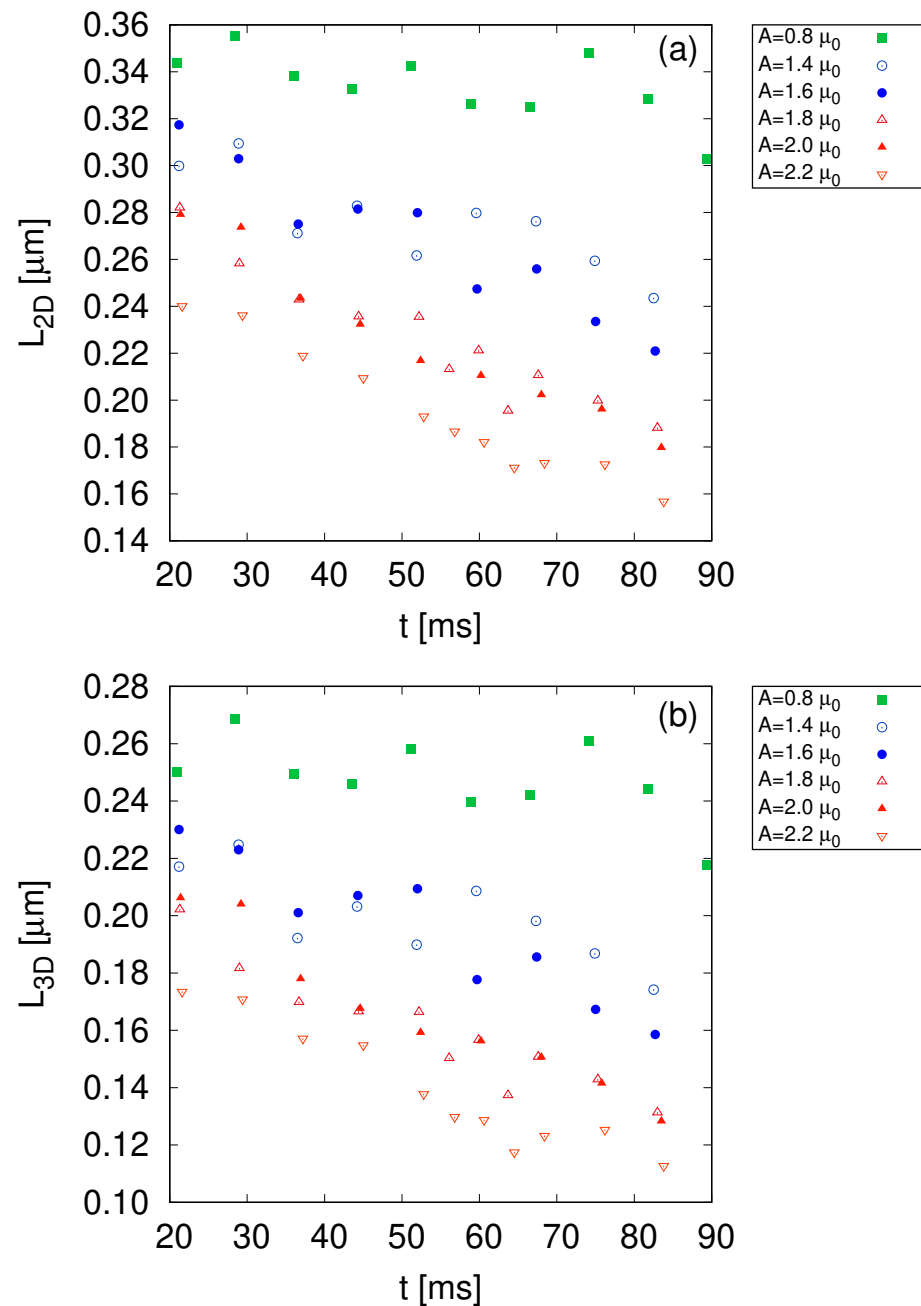


Figure 4. Time evolution of the characteristic length scale for different excitation amplitudes computed with (a) the two-dimensional projection of the cloud and (b) its three-dimensional reconstruction using the inverse Abel transform. Although the values computed with two-dimensional profiles are higher, their qualitative behavior is the same.

The characteristic length scale decreases with time, indicating the particle transfer to higher-momenta, but slower than the higher excitation amplitudes.

In this work and previous investigations [13], we identified the highest excitation amplitudes with turbulent clouds, $A = 1.8, 2.0$, and $2.2 \mu_0$. The value of $L(t)$ at the end of the processes seems to depend on the amplitude and, more importantly, if we deal with a moderate perturbation, the onset of turbulence, or a state with turbulent characteristics. It is interesting to observe that the turbulent states quickly reach lengths comparable to the healing length ($\xi_0 = 0.15(2) \mu\text{m}$), where dissipation processes are expected to occur.

The behavior of the characteristic length scale can be described by an exponential decay,

$$L(t) = L_0 \exp(-t/t_0), \quad (8)$$

where L_0 is the extrapolation of the characteristic length scale to the instant when the excitation was introduced, and t_0 is its characteristic time.

In Fig. 5 we present the values of L_0 and t_0 fitted to the functional form of Eq. (8) for different excitation amplitudes. We did not include the results for $A = 0.8 \mu_0$ since we obtain a value of $t_0 \approx 750$ ms, of the same order as the lifetime of the condensate.

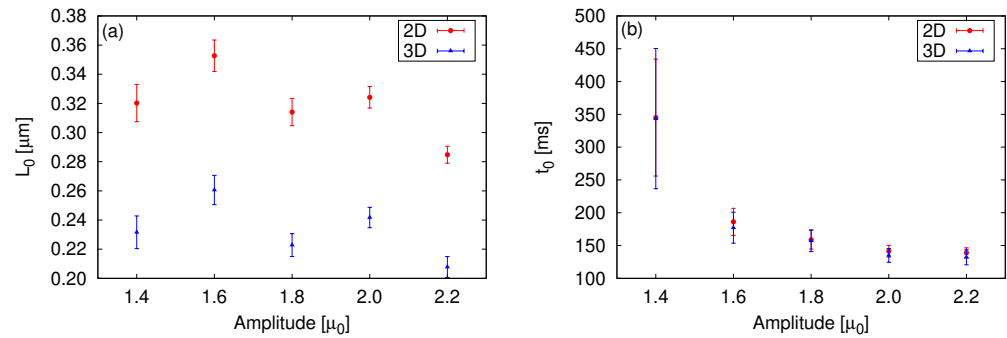


Figure 5. (a) Extrapolation of the characteristic length scale to the instant when the excitation is turned on, L_0 , and (b) the characteristic time of the particle transfer, t_0 , as a function of the excitation amplitude. The results were obtained fitting the data to the functional form of Eq. (8). Although the analysis employing two- or three-dimensional momentum distributions produces different values of L_0 , both approaches yield the same values for the characteristic time.

Figure 5(a) shows that the length containing most particles of the system is approximately the same with respect to the excitation amplitudes. However, if we perform the analysis employing the two- or three-dimensional momentum distributions, we arrive at different values for L_0 . A possible reason for this is that the inverse Abel transform slightly shifts the $n(k)$ profiles toward higher-momenta, see Fig. 3, which then implies a smaller value of L_0 .

In Fig. 5(b), we present the characteristic time that the particle transfer takes as a function of the excitation amplitude. It is observed that t_0 decreases with amplitude, as expected, since larger amplitudes lead to a faster formation of excitations and, therefore, speed up the decay. It is possible to see that the results obtained in 2D and 3D are in remarkable agreement. This opens the possibility of studying dynamical processes in 2D without the need to reconstruct the three-dimensional cloud, depending on the quantity of interest.

5. Discussion and final remarks

In this work, we defined and computed a characteristic length scale related to the momentum distribution of a trapped BEC, which allowed us to identify distinct out-of-equilibrium stages: a slightly perturbed cloud, the onset of turbulence, and the turbulent state. This quantity complements the formal analysis of identifying a power-law in the momentum distribution as a hallmark of turbulence.

We also focused our efforts on calculating this characteristic length scale using both two- and three-dimensional momentum distributions. The former is obtained straightforwardly from the experimental data, and the latter is reconstructed based on the symmetry of the cloud. From a technical point of view, it is preferable to work only with the two-dimensional distributions since no assumptions about the symmetry of the cloud have to be made. Although the length scales are affected by the inverse Abel transform, which shifts the momentum distributions to higher momenta, the qualitative behavior calculated in 2D and 3D is remarkably similar. The excellent agreement in the characteristic time of

the particle transfer indicates that the two-dimensional analysis may be appropriate to investigate dynamical aspects of these systems.

One important remark is that isotropy is assumed through Eq. (3) only for the kinetically dominated regions in Fourier space. Such an assumption can be made even for inhomogeneous cigar-shaped clouds. This is because such large-scale inhomogeneities affect only regions in Fourier space up to the order of $k \sim 2\pi/L_{\min}$, where L_{\min} is the smaller linear size of the cigar-shaped cloud. In a previous work [12] we studied the impact of anisotropy in the energy transfer during the evolution of turbulence in a trapped BEC. Like the integral length scale, the energy flux can also be computed from the kinetic energy spectrum. We found that the turbulent state can be identified and characterized in terms of the energy flux regardless if we employ the whole cloud or just a region close to the major axis of the expanded cloud. We should note that the axial trapping frequencies of this work and Ref. [12] are very close, however in this work, we employ a radial trapping frequency which is ≈ 0.7 smaller than the one used in Ref. [12]. Thus the BECs in this work are much less elongated and closer to a spherical shape than the ones in Ref. [12]. Therefore the range of validity for Eq. (3) is even larger than in previous works.

In future works, we intend to vary the excitation protocol to investigate the changes in the characteristic length. Since there is a compromise between the excitation amplitude and time [6,19,20], it may prove insightful to investigate situations where the same amount of energy is introduced in the system, but varying the time it takes to be injected from very slow inputs up to abrupt changes.

Author Contributions: Conceptualization, F.E.A.d.S. and V.S.B.; methodology, L.M.; software, L.M.; validation, L.M., A.D.G.-O., and M.A.M.-A; formal analysis, L.M.; investigation, L.M., A.D.G.-O., and M.A.M.-A; resources, V.S.B.; data curation, L.M., A.D.G.-O., and M.A.M.-A; writing—original draft preparation, L.M.; writing—review and editing, F.E.A.d.S. and V.S.B.; visualization, L.M.; supervision, V.S.B.; project administration, L.M.; funding acquisition, V.S.B. All authors have read and agreed to the published version of the manuscript.

Funding: This work was supported by the São Paulo Research Foundation (FAPESP) under the grants 2013/07276-1, 2014/50857-8, and 2018/09191-7, and by the National Council for Scientific and Technological Development (CNPq) under the grant 465360/2014-9. FEAS thanks CNPq (Conselho Nacional de Desenvolvimento Científico e Tecnológico, National Council for Scientific and Technological Development) for support through Bolsa de produtividade em Pesquisa Grant No. 305586/2017-3.

Acknowledgments: We thank L. Galantucci and C. Barenghi for the useful discussions.

Conflicts of Interest: The authors declare no conflict of interest.

Abbreviations

The following abbreviations are used in this manuscript:

QT	Quantum turbulence
BEC	Bose-Einstein condensate
TOF	Time-of-flight

Appendix A. The Abel transform

We used the inverse Abel transform to reconstruct a three-dimensional momentum distribution from its two-dimensional projection in the main text. It is insightful to take the inverse route to see what is the two-dimensional projection of a known three-dimensional $n_{3D}(k)$. In this appendix, we considered two relevant cases for our physical system that possess analytical solutions.

The Abel transform is given by

$$n_{2D}(k) = 2 \int_k^\infty dk' \frac{n_{3D}(k')k'}{\sqrt{k'^2 - k^2}}. \quad (A1)$$

The first case we considered is a Gaussian normalized according to Eq. (6),

$$n_{G;3D}(k) = \frac{\sqrt{2}}{\sqrt{\pi}\sigma^3} e^{-k^2/(2\sigma^2)}. \quad (A2)$$

Using Eq. (A1), the normalized two-dimensional projection is

$$n_{G;2D}(k) = \frac{1}{\sigma^2} e^{-k^2/(2\sigma^2)}. \quad (A3)$$

Hence, the Abel transform of a Gaussian is a Gaussian of the same width. This is very convenient in the case of the temperature of the cloud, for example, since it is estimated through the width of the Gaussian profile of the momentum distribution.

The second case we considered is a power-law with exponent δ_{3D} ,

$$n_{P;3D}(k) = Ak^{-\delta_{3D}}, \quad (A4)$$

with A constant. The standard normalization procedure, Eq. (6), is going to fail because this momentum distribution is not valid in the entire domain. In reality, the power-law would be observed over a certain k -range, $k_i \leq k \leq k_f$ with $k_i \neq 0$. However, this simplified example will have an interesting result as we will see. The Abel transformation yields

$$n_{P;2D}(k) = \frac{\sqrt{\pi}\Gamma\left(\frac{\delta_{3D}-1}{2}\right)}{\Gamma\left(\frac{\delta_{3D}}{2}\right)} Ak^{-(\delta_{3D}-1)} \equiv A'k^{-\delta_{2D}}, \quad (A5)$$

where Γ is the gamma function, A' is another constant, and $\delta_{2D} = \delta_{3D} - 1$. The conclusion is that the bidimensional projection of a power-law with an exponent of δ_{3D} in three-dimensions is also a power-law, but with the exponent increased by one.

Clearly, the momentum distributions we presented in the main text cannot be fully described by these two simple examples. However, they provide indications of the expected behavior of the projection procedure.

References

1. Tsatsos, M.C.; Tavares, P.E.; Cidrim, A.; Fritsch, A.R.; Caracanhas, M.A.; dos Santos, F.E.A.; Barenghi, C.F.; Bagnato, V.S. Quantum turbulence in trapped atomic Bose–Einstein condensates. *Phys. Rep.* **2016**, *622*, 1–52, [1512.05262]. doi:10.1016/j.physrep.2016.02.003.
2. Madeira, L.; Caracanhas, M.; dos Santos, F.; Bagnato, V. Quantum Turbulence in Quantum Gases. *Annu. Rev. Condens. Matter Phys.* **2020**, *11*, 37–56. doi:10.1146/annurev-conmatphys-031119-050821.
3. Madeira, L.; Cidrim, A.; Hemmerling, M.; Caracanhas, M.A.; dos Santos, F.E.A.; Bagnato, V.S. Quantum turbulence in Bose–Einstein condensates: Present status and new challenges ahead. *AVS Quantum Sci.* **2020**, *2*, 035901. doi:10.1116/5.0016751.
4. Madeira, L.; Bagnato, V.S. Cold Atoms Beyond Atomic Physics. *Brazilian J. Phys.* **2021**, *51*, 170–180. doi:10.1007/s13538-020-00805-3.
5. Henn, E.A.L.; Seman, J.A.; Roati, G.; Magalhães, K.M.F.; Bagnato, V.S. Emergence of Turbulence in an Oscillating Bose-Einstein Condensate. *Phys. Rev. Lett.* **2009**, *103*, 045301, [0904.2564]. doi:10.1103/PhysRevLett.103.045301.
6. Henn, E.A.L.; Seman, J.A.; Roati, G.; Magalhães, K.M.F.; Bagnato, V.S. Generation of Vortices and Observation of Quantum Turbulence in an Oscillating Bose-Einstein Condensate. *J. Low Temp. Phys.* **2010**, *158*, 435–442, [0910.2729]. doi:10.1007/s10909-009-0045-2.
7. Thompson, K.J.; Bagnato, G.G.; Telles, G.D.; Caracanhas, M.A.; dos Santos, F.E.A.; Bagnato, V.S. Evidence of power law behavior in the momentum distribution of a turbulent trapped Bose–Einstein condensate. *Laser Phys. Lett.* **2014**, *11*, 015501. doi:10.1088/1612-2011/11/1/015501.
8. Navon, N.; Gaunt, A.L.; Smith, R.P.; Hadzibabic, Z. Emergence of a turbulent cascade in a quantum gas. *Nature* **2016**, *539*, 72–75, [1609.01271]. doi:10.1038/nature20114.
9. Baggaley, A.W.; Barenghi, C.F.; Sergeev, Y.A. Three-dimensional inverse energy transfer induced by vortex reconnections. *Phys. Rev. E - Stat. Nonlinear, Soft Matter Phys.* **2014**, *89*, 013002. doi:10.1103/PhysRevE.89.013002.
10. Marino, Á.V.M.; Madeira, L.; Cidrim, A.; dos Santos, F.E.A.; Bagnato, V.S. Momentum distribution of Vinen turbulence in trapped atomic Bose–Einstein condensates. *Eur. Phys. J. Spec. Top.* **2021**, *230*, 809–812, [2005.11286]. doi:10.1140/epjs/s11734-021-00083-3.

11. Navon, N.; Eigen, C.; Zhang, J.; Lopes, R.; Gaunt, A.L.; Fujimoto, K.; Tsubota, M.; Smith, R.P.; Hadzibabic, Z. Synthetic dissipation and cascade fluxes in a turbulent quantum gas. *Science* **2019**, *366*, 382–385, [1807.07564]. doi:10.1126/science.aau6103.
12. Daniel García-Orozco, A.; Madeira, L.; Galantucci, L.; Barenghi, C.F.; Bagnato, V.S. Intra-scales energy transfer during the evolution of turbulence in a trapped Bose-Einstein condensate. *EPL (Europhysics Lett.)* **2020**, *130*, 46001, [2002.01267]. doi:10.1209/0295-5075/130/46001.
13. Madeira, L.; García-Orozco, A.D.; dos Santos, F.E.A.; Bagnato, V.S. Entropy of a Turbulent Bose-Einstein Condensate. *Entropy* **2020**, *22*, 956. doi:10.3390/e22090956.
14. Cidrim, A.; White, A.C.; Allen, A.J.; Bagnato, V.S.; Barenghi, C.F. Vinen turbulence via the decay of multicharged vortices in trapped atomic Bose-Einstein condensates. *Phys. Rev. A* **2017**, *96*, 023617. doi:10.1103/PhysRevA.96.023617.
15. Bewley, G.P.; Lathrop, D.P.; Sreenivasan, K.R. Superfluid helium: Visualization of quantized vortices. *Nature* **2006**, *441*, 588. doi:10.1038/441588a.
16. Batchelor, G.K.; Press, C.U. *The Theory of Homogeneous Turbulence*; Cambridge Science Classics, Cambridge University Press, 1953.
17. WANG, H.; GEORGE, W.K. The integral scale in homogeneous isotropic turbulence. *J. Fluid Mech.* **2002**, *459*, 429–443. doi:10.1017/S002211200200811X.
18. Stagg, G.W.; Parker, N.G.; Barenghi, C.F. Ultraquantum turbulence in a quenched homogeneous Bose gas. *Phys. Rev. A* **2016**, *94*, 053632, [1607.03719]. doi:10.1103/PhysRevA.94.053632.
19. Seman, J.A.; Henn, E.A.; Shiozaki, R.F.; Roati, G.; Poveda-Cuevas, F.J.; Magalhães, K.M.; Yukalov, V.I.; Tsubota, M.; Kobayashi, M.; Kasamatsu, K.; Bagnato, V.S. Route to turbulence in a trapped Bose-Einstein condensate. *Laser Phys. Lett.* **2011**, *8*, 691–696. doi:10.1002/lapl.201110052.
20. Shiozaki, R.; Telles, G.; Yukalov, V.; Bagnato, V. Transition to quantum turbulence in finite-size superfluids. *Laser Phys. Lett.* **2011**, *8*, 393–397. doi:10.1002/lapl.201110005.
21. Caracanhas, M.; Fetter, A.L.; Baym, G.; Muniz, S.R.; Bagnato, V.S. Self-similar Expansion of a Turbulent Bose-Einstein Condensate: A Generalized Hydrodynamic Model. *J. Low Temp. Phys.* **2013**, *170*, 133–142. doi:10.1007/s10909-012-0776-3.
22. Hickstein, D.D.; Gibson, S.T.; Yurchak, R.; Das, D.D.; Ryazanov, M. A direct comparison of high-speed methods for the numerical Abel transform. *Rev. Sci. Instrum.* **2019**, *90*, 065115, [1902.09007]. doi:10.1063/1.5092635.